Chemical Reactions-Based Microfluidic Transmitter and Receiver Design for Molecular Communication

Dadi Bi, *Student Member, IEEE*, Yansha Deng, *Member, IEEE*, Massimiliano Pierobon, *Member, IEEE*, and Arumugam Nallanathan, *Fellow, IEEE*

Abstract—The design of communication systems capable of processing and exchanging information through molecules and chemical processes is a rapidly growing interdisciplinary field, which holds the promise to revolutionize how we realize computing and communication devices. While molecular communication (MC) theory has had major developments in recent years, more practical aspects in designing components capable of MC functionalities remain less explored. This paper designs chemical reactions-based microfluidic devices to realize binary concentration shift keying (BCSK) modulation and demodulation functionalities. Considering existing MC literature on information transmission via molecular pulse modulation, we propose a microfluidic MC transmitter design, which is capable of generating continuously predefined pulse-shaped molecular concentrations upon rectangular triggering signals to achieve the modulation function. We further design a microfluidic MC receiver capable of demodulating a received signal to a rectangular output signal using a thresholding reaction and an amplifying reaction. Our chemical reactions-based microfluidic molecular communication system is reproducible and its parameters can be optimized. More importantly, it overcomes the slow-speed, unreliability, and non-scalability of biological processes in cells. To reveal design insights, we also derive the theoretical signal responses for our designed microfluidic transmitter and receiver, which further facilitate the transmitter design optimization. Our theoretical results are validated via simulations performed through the COMSOL Multiphysics finite element solver. We demonstrate the predefined nature of the generated pulse and the demodulated rectangular signal together with their dependence on design parameters.

Index Terms—Molecular communication, microfluidics, microfluidic transmitter, microfluidic receiver, chemical reaction, chemical circuits, genetic circuits.

I. INTRODUCTION

THE possibility of harnessing information processing and communication functionalities from physical and chemi-

Dadi Bi and Yansha Deng are with the Department of Engineering, King's College London, London WC2R 2LS, U.K. (e-mail: dadi.bi@kcl.ac.uk; yansha.deng@kcl.ac.uk).

Massimiliano Pierobon is with the Department of Computer Science and Engineering, University of Nebraska–Lincoln, Lincoln, NE 68588 USA (e-mail: pierobon@cse.unl.edu).

Arumugam Nallanathan is with the School of Electronic Engineering and Computer Science, Queen Mary University of London, London E1 4NS, U.K. (e-mail: a.nallanathan@qmul.ac.uk).

cal processes at the level of molecules has been at the basis of a great bulk of research in recent years on Molecular Communication (MC) [2]–[4]. The physical processes of molecule propagation usually include diffusion and convection, which govern the molecule transport and can usually be described by a convection-diffusion equation [5], [6]. Meanwhile, chemical reactions may occur during molecule propagation via enzyme reaction [7], or at the reception of molecule via reversible absorption reaction [8] or ligand binding reaction [9]. To capture the molecule behaviour at any time, existing research has mainly focused on mathematically modelling and theoretical analysis of these physical and chemical processes, such as the channel response modelling [8], [10], channel capacity calculation [11], [12], and bit error probability derivation [7], [13].

Despite substantial research outcomes in the above theoretical study, the design and prototyping of components with MC functionalities has been less explored except from some works [1], [14]–[19], partly because of the highly interdisciplinary technical knowledge and tools required to engineer these systems in practice. Existing MC prototypes can be classified into macroscale MC prototypes [14]–[16] and nanoscale or microscale MC prototypes [1], [17]–[19]. The macroscale testbeds in [14]–[16] considered the information sharing over a distance via alcohol and odor particles, but these macroscale testbeds are inapplicable or inappropriate to be operated in very small dimensions or in specific environment, such as in the water or in the human body. Besides, the detection of signaling molecules heavily relies on electrical devices, including sensors and mass spectrometry (MS), where the signal processing over chemical signals has been less explored in the molecular domain.

For microscale MC testbeds, the authors in [17] proposed a Hydrodynamic Controlled Microfluidic Network (HCN) and demonstrated how to realize a pure hydrodynamic microfluidic switching function, where the successful routing of payload droplets was achieved by designing the geometry of microfluidic circuits. In [18], the genetically engineered *Escherichia coli* (*E. coli*) bacteria, housed in a chamber inside a microfluidic device, serves as an MC receiver using fluorescence detection upon the receipt of the signaling molecule C6-HSL. Note that the microfluidic channel in [18] was only used as a propagation pathway for C6-HSL molecule, and the authors did not analytically evaluate the response of the C6-HSL molecule transport inside microfluidics. Furthermore, the microfluidic designs in [17], [18] did not realize any signal processing functions, such as modulation and demodulation, in molecular domain.

Signal processing functions performed over electrical signals or devices usually involves a highly complex procedure, and the utilization of electrical devices faces challenges, such as lack of biocompatibility and invasiveness, for biomedical-related applications [4]. This motivates us to perform signal processing directly over chemical signals. In general, signal processing functions over chemical signals can be achieved using two approaches: 1) biological circuits [20] in engineered living cells, and 2) chemical circuits [21] based on "non-living" chemical reactions. Existing works in [19] have already designed biological circuits to realize the parity-check encoder and decoder. However, the utilization of biological cells for MC currently faces challenges such as slow speed, unreliability, and non-scalability, which motivates our initial work [1].

In our previous work, we designed a chemical reactions-based microfluidic transmitter for MC [1], which is motivated by a bulk of MC literature on information transmission via *concentration shift keying (CSK)* modulation [4], [22] and inspired by how cells generate pulse-shaped molecular signals in biology [23]. Our proposed transmitter is capable of generating a molecular concentration pulse upon a rectangular signal, thus realizing the modulation function. One relevant microfluidic MC work was presented in [24], where they theoretically analyzed the expected time course of bound receptor concentration based on a two-compartment model. Unlike that chemical reactions happen anywhere during the propagation inside reactions channels in [1], the ligand-binding reaction only occurs on a reaction surface placed at the bottom of a microfluidic channel. In other words, the analysis obtained from [24] relying on a different boundary condition for reactive surface receiver, and a different differential equation for propagation. Although the theoretical analysis in [1] and [24] both capture the effect of microfluidic channel and receiver geometry, a further optimization design of the microfluidic devices was not investigated.

The objective of this paper is to continue exploring modulation and demodulation abilities of microfluidic devices via chemical reactions. Different from [1], [24], we further optimize our previous transmitter design and propose a novel microfluidic receiver design. The optimized transmitter modulates rectangular digital inputs to pulse-shaped signals, which is analogous to the *Amplitude Shift Keying (ASK)* modulation in wireless communication. Instead of directly emitting the digital inputs, the maximum concentrations of the modulated pulses can be tuned according to our optimization. This enables us to transmit multiple symbols using different maximum concentrations, which may improve the data rate. Our proposed microfluidic receiver demodulates a received pulse to a rectangular-shaped signal that has a steep transition between minimum and maximum concentrations. The digital characteristic of the rectangular-shaped digital signals allows either the transmitter or receiver to further incorporate Boolean computations to generate customized behaviours [25]. Our main contributions are listed as follows:

- We first optimize our previous microfluidic transmitter design [1]. We present a reaction channel length optimization framework to guide how to tune the maximum concentration of a generated pulse. We also analyse the restricted time gap between two consecutive input signals to ensure a continuous transmission of non-distorted pulses.
- We then propose a microfluidic receiver design capable of demodulating a received signal to a rectangular output signal. This demodulation is realized via two chemical reactions, where a thresholding reaction is proposed to first deplete the received signal below the threshold, and an amplifying reaction converts the residual received signal into a digital output.
- Unlike [18], we address a new challenge in mathematically modelling the dynamics of molecular species in microfluidic channels, which is deriving the channel response of the straight convection-diffusion-reaction channels. Although only rectangular and Gaussian input concentrations are considered, our methodology can be used for any concentration profiles. Importantly, the analytical results are validated via the simulations performed in the COMSOL Multiphysics finite element solver.

We highlight that our proposed transmitter and receiver design not only constitutes a simple end-to-end MC system, but also brings new opportunities for certain applications. For example, our transmitter design can act as a concentration gradient generator (CGG) to investigate the role of concentration gradients in cell development, inflammation, and wound healing [26], while our receiver can be attached to field-deployable biosensors to detect chemical and biological threats [27].

The rest of the paper is organized as follows. In Sec. II, we present the microfluidic transmitter and receiver design in terms of chemical reactions and microfluidic components. In Sec. III, we introduce microfluidic characteristics and theoretically analyse convection-diffusion channels and convection-diffusion-reaction channels. In Sec. IV and V, we not only present the analysis and design for the proposed microfluidic transmitter and receiver, respectively, but also provide numerical simulation results performed in COMSOL Multiphysics. In Sec. VI, we combine the microfluidic transmitter with the receiver to show a basic end-to-end MC system. Finally, Sec. VII concludes the paper.

II. System Model

The overall scheme of the proposed transmitter and receiver for MC is shown in Fig. 1. At the microfluidic transmitter, a high digital rectangular input molecular signal composed of the molecular species X in a fluid with concentration $C_X(t)$ enters the microfluidic transmitter that upon a variation in $C_X(t)$ produces an output molecular signal composed of molecular species Y with concentration $C_Y(t)$ by following a predefined pulse shape. After convection-diffusion of the emitted pulse $C_Y(t)$, a microfluidic receiver is designed to demodulate the received pulse to a rectangular output signal using species O with concentration $C_O(t)$. Here, both the pulse shape and the demodulated signal shape are dependent on the values of parameters in the microfluidic device implementation. As the fluids flow through microfluidic device channels, a series of chemical reactions occur to generate the molecules of species Y and species O, which guarantee
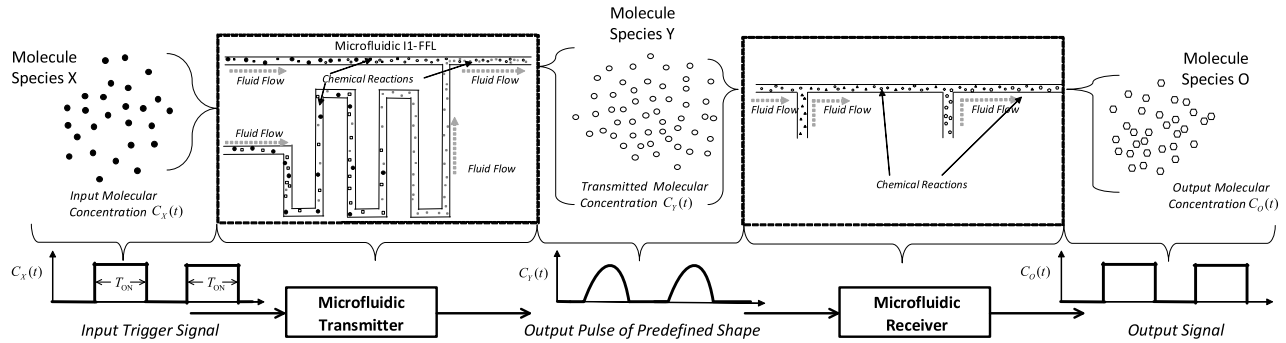
Fig. 1.   Overall scheme of the proposed transmitter and receiver for MC.

the successful pulse generation and the signal demodulation. In the following, we first introduce these chemical reactions at the transmitter side and receiver side, and then describe the microfluidic components of the transmitter and receiver.

A. Chemical Reactions Design for the Microfluidic MC Devices

1) Chemical Reactions Design for the Microfluidic Transmitter: Gene regulatory networks are sets of interconnected biochemical processes in a biological cell [28], where DNA genes are linked together by activation and repression mechanisms of certain biological macromolecules that regulate their expressions into proteins. Each DNA gene contains coding sequences and regulatory sequences, which are sites the proteins (transcription factor) can bind and control the rate of the gene expression, either by increasing (activation) or decreasing (repression) the rate of protein synthesis. In gene regulatory networks, genes are interconnected such that the proteins produced by one or more genes regulate the expression of one or more genes, which results in complex protein expression dynamics.

Gene regulatory networks can be abstracted with nodes representing the genes, interconnected by directed edges that correspond to the control of a gene (edge destination) expression by a transcription factor encoded by another gene (edge source). Network motifs are patterns of nodes and directed edges that occur more frequently in natural gene transcription networks than randomized networks [29]. The Feed Forward Loop (FFL) is a family of network motifs among all three-node patterns frequently observed in nature [23], [29]. In the structure of FFL, the transcription factor protein X regulates the genes expressing other two proteins, namely, P and Y, where P is also a transcription factor that regulates the gene expressing protein Y. Depending on the types of these regulations, either activation or repression, there are 8 different FFLs [30].

Among all the FFLs found in nature, the I1-FFL results in a pulse-like dynamics of its output Y [23]. As shown in Fig. 2, an input gene expresses the protein X, which is a transcription factor for the genes expressing Y and P. In the presence of X, the expressions of the genes encoding protein Y and protein P are activated, resulting in the build up of the concentrations of protein Y and protein P, respectively. On its turn, the protein
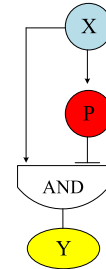

Fig. 2.   The I1-FFL network motif.

P is another transcription factor that works as a repressor for the gene encoding protein Y. The AND input to the gene that encodes Y corresponds to a situation where this gene is activated when the transcription factor X binds to the regulatory sequence, but it is inactivated whenever transcription factor P binds to the same sequence independently from the presence of X. In such a way, protein X initializes the rapid expression of the gene encoding protein Y first, and after a delay, enough P accumulates and represses the production of protein Y, whose concentration will continuously decrease because of natural degradation. This generates a pulse shape for the concentration of protein Y as a function of the time.
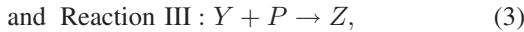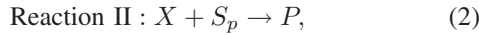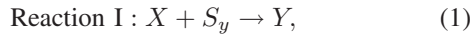
One example of I1-FFL is the galactose system of *E. coli*, where the galactose utilization operon (a cluster of genes sharing the same regulatory sequences and expressed together) *gal*ETK is regulated in an I1-FFL fashion by the activator CRP (X), and the repressor *galS* (P) [31]. Results showed that in nature we can observe a pulse-like expression of the *gal*ETK genes, which is initiated by a step variation of active CRP mediated by the molecular species $cAMP$.

In this paper, we take inspiration from the I1-FFL to design a transmitter in the molecular domain. Although the discipline of synthetic biology is opening the road to the programming of functionalities in the biochemical environment through genetic engineering of biological cells [32], there are a number of factors that suggest an alternative technology for the design of an MC transmitter in this paper, such as the small number of molecules involved for each cell together with difficulties in coordinating multiple cells, the added complexity of cellular behavior, including cell growth, evolution, and biological noise, and the slow response time of genetic regulatory

networks such as the I1-FFL, whose output pulse shape is usually realized in nature in the order of cell generation time (hours) as indicated in [31, Fig. 4].

Inspired by the I1-FFL mechanism in gene regulation networks, we explore the realization of I1-FFL via mass action chemical reactions, *i.e.*, processes that convert one or more input molecules (*reactants*) into one or more output molecules (*products*). Reactions may proceed in forward or reverse directions, which are characterized by forward (k_f) and reverse (k_r) reaction rates, respectively. Within the scope of this paper, we assume unbalanced reactions where the forward reaction rate is much greater than the reverse rate. A chemical reaction network is defined as a finite set of reactions involving a finite number of species [21], where these reactions occur in a well-stirred environment, aiming to realize a function or algorithm via mass action chemical reactions. Specific chemical reaction networks have already been designed for signal restoration, noise filtering, and finite automata, respectively, through a discipline known as molecular programming [33].

To execute the same functionality of an I1-FFL with a chemical reaction network, we define three chemical reactions as follows:

$$\text{Reaction I}: X + S_y \rightarrow Y, \tag{1}$$

$$\text{Reaction II}: X + S_p \rightarrow P, \tag{2}$$

$$\text{and Reaction III}: Y + P \rightarrow Z, \tag{3}$$

where these reactions involve the input molecular species X, the molecular species S_p and S_y, the intermediate product molecular species P, and the output molecular species Y.

In the I1-FFL gene regulation network, the active X first activates the gene expressing the protein Y, and only when P accumulates sufficiently, it suppresses the expression of the protein Y, generating the aforementioned pulse-like concentration signal. Here, the molecular species X, S_p, and S_y are only injected at $t = 0$, and the chemical reactions in (1), (2), and (3) happen simultaneously with a much quicker speed under well-stirred environment than that of the I1-FFL gene regulation network dynamics, which may not result in the pulse-like output signal Y when these three reactions have the same reaction rate. One way to cope with it is to adjust the reaction rates to be different among these reactions.

However, in practice, we want to design the molecular communication system modulation with the pulse-like output triggered by the rectangular pulse input representing bit-1 transmission. In such a way, the output pulse only occurs inside the duration of a rectangular pulse input, and all bits are modulated to their corresponding pulses as shown in Fig. 1. To control the rectangular pulse input signals, the sequence of each reaction, and the delayed arrival of product P after Reaction II in (2), we propose a microfluidic transmitter to realize the same functionality of I1-FFL as in gene regulation network in Fig. 3 and containing the reactions (1), (2), and (3).

2) Chemical Reactions Design for the Microfluidic Receiver: According to the demodulation requirement of traditional communication systems, we aim to design a microfluidic receiver capable of demodulating the received pulse to a rectangular signal. To do so, we design the chemical reactions as follows:

$$\text{Reaction IV}: Y + ThL \rightarrow Waste, \tag{4}$$

$$\text{and Reaction V}: Y + Amp \rightarrow Y + O, \tag{5}$$
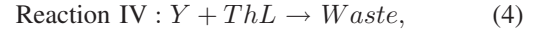
where these reactions involve the input molecular species Y, the molecular species ThL and Amp, intermediate product molecular species $Waste$, and the output molecular species O. Once the species Y arrives at the receiver, the Reaction IV is immediately activated, resulting in a depletion of species Y that is below the concentration of species ThL. Then, any remaining Y catalyses the conversion of species Amp into the output species O. Obviously, output species O will only be produced when the concentration of Y is greater than the concentration of ThL, so we regard the concentration of ThL as a threshold and name Reaction IV as the thresholding reaction. Reaction V refers to an amplifying reaction. Similar to the chemical reactions at the transmitter, the sequence of Reaction IV and Reaction V is controlled by the microfluidic receiver geometry design, which will be presented next.

We note that Reaction V is necessary and we detect species O instead of species Y. The reasons are as follows. First, the remaining concentration of species Y may not reach the minimum detectable level of a detector. With Reaction V, the output can satisfy a detector's sensitivity via adjusting the injected concentration of species Amp. Second, Reaction V is performed to generate the output to be a rectangular digital signal, which can allow our receiver to link post Boolean computation modules [25]. One example is to perform an AND operation for multiple outputs to further enhance biosensors' specificity [34].

B. Microfluidic Device Design

In this subsection, we describe each component of our proposed microfluidic transmitter and receiver, in Fig. 3. A microfluidic device is a system that can process or manipulate small (10^{-9} to 10^{-18} litres) amount of fluids using channels in dimensions of tens to hundreds of micrometres [27]. Recently, an increasing number of biological and chemical experiments are conducted in microfluidic or lab-on-a-chip (LOC) devices, due to inherent advantages in miniaturization, integration, portability and automation with low reagents consumption, rapid analysis, and high efficiency [35]. According to whether a chemical reaction occurs in a microfluidic channel, we classify microfluidic components as two types: 1) convection-diffusion channel, and 2) convection-diffusion-reaction channel.

1) Convection-Diffusion Channel:

- **Y Junction at the microfluidic transmitter:** The reactions between reactants require mixing to occur in a short distance, which can be facilitated by convection-diffusion in Y junctions. Y junctions are configured by one outlet and two inlets, *i.e.*, Y junction I and Y junction II in Fig. 3, where the outlet width is doubled compared with each inlet width, and the angle between the main channel and the first inlet starting anticlockwise from the main channel is 145°. The fluid flow containing
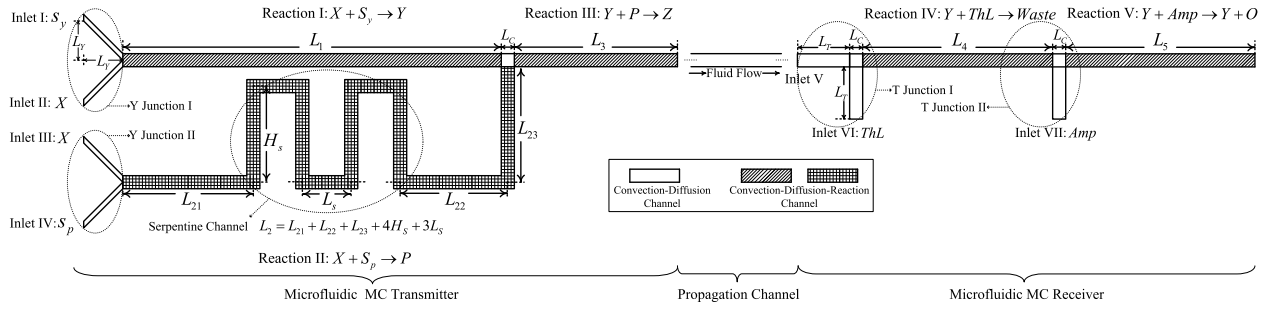
Fig. 3. Novel design of the microfluidic MC transmitter and receiver.

input reactant X with concentration $C_{X_0}^{II}$ and $C_{X_0}^{III}$ is injected into the Inlet II and Inlet III using syringe pumps, which can be described by a rectangular pulse signal, as in Fig. 1, with the value of the width equalling to the length of injection time T_{ON}, whereas the reactant S_y with concentration $C_{S_{y_0}}^{I}$ and reactant S_p with concentration $C_{S_{p_0}}^{IV}$ are continuously injected into Inlet I and Inlet IV, respectively. By doing so, the flows from Inlet I and Inlet IV can flush the microfluidic device continuously without influencing Reaction III in (3).

- **T Junction at the microfluidic receiver:** T junctions are chosen at the receiver equipping with the same functionality as Y junctions. A T Junction has one outlet and two inlets, *i.e.*, T junction I and T junction II in Fig. 3, where the angle between the second inlet starting anti-clockwise from the first inlet is 90°, and one inlet of T junction II is merged into a convection-diffusion-reaction channel. After diffusion, the transmitted molecules from microfluidic transmitter propagate to enter the receiver, and the reactant ThL with concentration C_{ThL}^{VI} and Amp with concentration C_{Amp}^{VII} are continuously injected into the Inlet VI and Inlet VII, respectively.

- **Straight Convection-Diffusion Channel:** This channel is used to connect the transmitter with the receiver and provides a propagation pathway for a generated pulse.

2) Convection-Diffusion-Reaction Channel: For simplicity, in the following, we refer to the channel in which Reaction i happens as the Reaction i channel.

- **Transmitter**
  Straight Reaction I Channel: The outflow of Y junction I passes through the Reaction I channel with length L_1 to realize the Reaction I in (1) to generate the output signal Y.
  Serpentine Reaction II Channel: The outflow of Y junction II passes through the Reaction II channel to generate P according to the Reaction II in (2). To realize the pulse-shaped concentration of emitted signal Y, the Reaction II channel is designed to be longer than the Reaction I channel, with the result of delaying the contact between species P and Y, and therefore delaying the Reaction III. Furthermore, a serpentine channel is designed and replaced a straight reaction channel to delay the arrival of species P in a compact space within the microfluidic transmitter. The width and height of the serpentine

channel is denoted as L_s and H_s, respectively. The design in Fig. 3 is conventionally denoted as containing 2 delay lines, due to its two bended tubes with height H_s in the serpentine channel. The equivalent straight channel length of this serpentine channel is denoted as L_2 and can be calculated as $L_2 = L_{21} + L_{22} + L_{23} + 4H_s + 3L_s$.
  Straight Reaction III Channel: Once P arrives at the Reaction III channel with length L_3, Reaction III in (3) occurs to decrease the output signal Y.

- **Receiver**
  Straight Reaction IV Channel: The outflow of T junction I flows through the Reaction IV channel with length L_4 to deplete Y below the concentration of species ThL according to Reaction IV in (4).
  Straight Reaction V Channel: When the remaining Y arrives at the Reaction V channel with length L_5, Reaction V in (5) is activated to convert the species Amp into output species O.

III. BASIC MICROFLUIDIC CHANNEL ANALYSIS

In this section, we first describe the basic characteristics of microfluidics, and then use 1D model to approximate and derive analytical expressions for convection-diffusion channels and convection-diffusion-reaction channels. Numerical results are provided to verify our theoretical analysis.

A. Basic Characteristics of Microfluidics

The nature of the flow highly depends on the Reynolds number, which is the most famous dimensionless parameter in fluid mechanics. For flow in a pipe, the Reynolds number is defined as [6]

$$\text{Re} = \frac{\rho v_{\text{eff}} D_H}{\mu}, \qquad (6)$$

where ρ is the fluid density, v_{eff} is the fluid mean velocity, D_H is the hydraulic diameter of the channel, and μ is the constant fluid viscosity. When we scale down standard laboratory channels from decimeter scale to microscopic scale, Reynolds number is usually very small ($\text{Re} < 1$), which indicates that flows become laminar flows, such that an ordered and regular streamline pattern can be experimentally observed [36]. Applying a long, straight, and rigid microfluidic channel to a flow and imposing a pressure difference between the two ends of the channel, the flow is referred to as the Poiseuille

flow. When the cross section of the microfluidic channel is rectangular-shaped with height h and width w, the flow velocity profile can be described as

$$v(y,z) = \frac{4h^2\Delta p}{\pi^3 \mu l}\sum_{n,\text{odd}}^{\infty}\frac{1}{n^3}[1 - \frac{\cosh(\frac{n\pi y}{h})}{\cosh(\frac{n\pi w}{2h})}]\sin(\frac{n\pi z}{h}), \quad (7)$$

where $\Delta p/l$ denotes the pressure difference between two ends of a microfluidic channel with length l [6].

B. Convection-Diffusion Channels

For one type of molecular species flowing in a 3D straight convection-diffusion channel with rectangular cross section, its concentration $C(x,y,z,t)$ can be described by the 3D convection-diffusion equation as [37]

$$\frac{\partial C(x,y,z,t)}{\partial t} = D\nabla^2 C(x,y,z,t) - \boldsymbol{v}\cdot\nabla C(x,y,z,t), \quad (8)$$

where ∇ is the Nabla operator, and $\boldsymbol{v}$ is the flow velocity described by (7). When the flow falls into dispersion regime, the interaction between cross-sectional diffusion and non-uniform convection can lead to a uniform molecule distribution along the cross-section, i.e., $\frac{\partial C(x,y,z,t)}{\partial y} = \frac{\partial C(x,y,z,t)}{\partial z} = 0$, such that (8) can be simplified into a 1D convection-diffusion equation [38]

$$\frac{\partial C(x,t)}{\partial t} = D_{\text{eff}}\frac{\partial^2 C(x,t)}{\partial x^2} - v_{\text{eff}}\frac{\partial C(x,t)}{\partial x}, \quad (9)$$

where $D_{\text{eff}} = (1 + \frac{8.5 v_{\text{eff}}^2 h^2 w^2}{210 D^2(h^2 + 2.4hw + w^2)})$ is the *Taylor-Aris* effective diffusion coefficient [39].

C. Convection-Diffusion-Reaction Channels

Unlike a convection-diffusion channel, the molecular transport is not only affected by convection-diffusion, but also affected by reactions in a reaction channel. To quantitatively describe the chemical reaction and dispersion of molecules at a straight microfluidic channel, we use the 1D convection-diffusion-reaction equation. For a general reaction $A + B \rightarrow AB$, the spatial-temporal concentration distribution of species A and AB can be described as

$$\frac{\partial C_A(x,t)}{\partial t} = D_{\text{eff}}\frac{\partial^2 C_A(x,t)}{\partial x^2} - v_{\text{eff}}\frac{\partial C_A(x,t)}{\partial x} - kC_A(x,t)C_B(x,t), \quad (10)$$

$$\frac{\partial C_{AB}(x,t)}{\partial t} = \underbrace{D_{\text{eff}}\frac{\partial^2 C_{AB}(x,t)}{\partial x^2}}_{\text{Diffusion}} - \underbrace{v_{\text{eff}}\frac{\partial C_{AB}(x,t)}{\partial x}}_{\text{Convection}} + \underbrace{kC_A(x,t)C_B(x,t)}_{\text{Reaction}}, \quad (11)$$

where k is the rate constant. Assuming species B with concentration C_{B_0} is continuously injected at the inlet of the channel at $x = 0$ and $t = 0$ with velocity v_{eff}, we solve the above convection-diffusion-reaction equations in the following two theorems, when species A is injected with a rectangular and Gaussian concentration profiles as they are considered as the inputs of the transmitter and receiver later.

Theorem 1: With species A following a rectangular concentration distribution

$$C_A(0,t) = C_{A_0}[u(t) - u(t - T_{\text{ON}})] \quad (12)$$

being injected at the inlet of a straight microfluidic channel at $x = 0$ and $t = 0$ using velocity v_{eff}, the concentration distributions of A and AB are derived as

$$C_A(x,t) = \begin{cases} g(x,t), & 0 \leq t \leq T_{\text{ON}} \\ g(x,t) - g(x, t - T_{\text{ON}}), & t > T_{\text{ON}}, \end{cases} \quad (13)$$

and

$$C_{AB}(x,t)$$
$$= \begin{cases} h(x,t) - g(x,t), & \\ & 0 \leq t \leq T_{\text{ON}}, \\ [h(x,t) - g(x,t)] - [h(x, t - T_{\text{ON}}) - g(x, t - T_{\text{ON}})], & \\ & t > T_{\text{ON}}, \end{cases} \quad (14)$$

where $u(t)$ is the Heaviside step function,

$$h(x,t) = \frac{C_0}{2}[\text{erfc}(\frac{x - v_{\text{eff}}t}{2\sqrt{D_{\text{eff}}t}}) + e^{\frac{v_{\text{eff}}x}{D_{\text{eff}}}}\text{erfc}(\frac{x + v_{\text{eff}}t}{2\sqrt{D_{\text{eff}}t}})], \quad (15)$$

$$and \quad g(x,t) = \frac{C_0}{2}\left\{\exp\left[\frac{(v_{\text{eff}} - \alpha)x}{2D_{\text{eff}}}\right]\text{erfc}\left[\frac{x - \alpha t}{2\sqrt{D_{\text{eff}}t}}\right] + \exp\left[\frac{(v_{\text{eff}} + \alpha)x}{2D_{\text{eff}}}\right]\text{erfc}\left[\frac{x + \alpha t}{2\sqrt{D_{\text{eff}}t}}\right]\right\} \quad (16)$$

with $C_0 = \min\{C_{A_0}, C_{B_0}\}$ and $\alpha = \sqrt{v_{\text{eff}}^2 + 4kC_0 D_{\text{eff}}}$.
Proof: See the Appendix A. □
Theorem 2: With species A following a Gaussian concentration distribution

$$C_A(0,t) = \frac{C_{A_0}}{\sqrt{2\pi\sigma^2}}e^{-\frac{(t-\mu)^2}{2\sigma^2}} \quad (17)$$

being injected at the inlet of a straight microfluidic channel at $x = 0$ and $t = 0$ using velocity v_{eff} and $C_{B_0} < \max\{C_A(0,t)\}$, the concentration distribution of species A, i.e., $C_A(x,t)$, can be approximated as

$$C_A^{\text{Appro1}}(x,t)$$
$$= \begin{cases} C_A(0, t - \frac{x}{v_{\text{eff}}}) - C_{B_0}, & t_1 + \frac{x}{v_{\text{eff}}} \leq t \leq t_2 + \frac{x}{v_{\text{eff}}}, \\ 0, & \text{otherwise}, \end{cases} \quad (18)$$

$$or \quad C_A^{\text{Appro2}}(x,t)$$
$$= \frac{1}{2\pi}\int_0^{\infty}[e^{-j\omega t}\widetilde{C_A^{\text{Appro2}}}(x,\omega) + e^{j\omega t}\widetilde{C_A^{\text{Appro2}}}(x,\omega)]\mathrm{d}w, \quad (19)$$
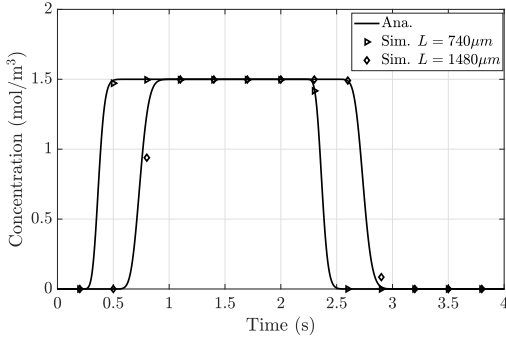
Fig. 4. The concentration of species AB in **Theorem 1** with different channel length L.

Fig. 5. The concentration of species A in **Theorem 2** with $L = 540\mu$m and different C_{B_0}.

where

$$\widetilde{C_A^{\text{Appro}_2}}(x, s) = l(s)e^{\frac{v_{\text{eff}} - \sqrt{v_{\text{eff}}^2 + 4D_{\text{eff}} s}}{2D_{\text{eff}}}x}, \tag{20}$$

$$l(s) = C_{A_0} e^{-s\mu + \frac{(\sigma s)^2}{2}}[Q(\frac{t_1 + \sigma^2 s - \mu}{\sigma})$$
$$- Q(\frac{t_2 + \sigma^2 s - \mu}{\sigma})]$$
$$- \frac{C_{B_0}}{s}(e^{-st_1} - e^{-st_2}), \tag{21}$$

$$t_1 = \mu - \sqrt{-2\sigma^2 \ln\frac{C_{B_0}\sqrt{2\pi\sigma^2}}{C_{A_0}}}, \tag{22}$$

$$and\ t_2 = \mu + \sqrt{-2\sigma^2 \ln\frac{C_{B_0}\sqrt{2\pi\sigma^2}}{C_{A_0}}}. \tag{23}$$

Proof: See the Appendix B. $\square$

Our result $C_A^{\text{Appro}_2}(x, t)$ can be easily computed using Matlab. Importantly, (13), (18), and (19) reduce to solutions of a convection-diffusion equation when $C_{B_0} = 0$.

In Fig. 4 and 5, we plot the analytical outlet concentrations of species AB in **Theorem 1**, species A in **Theorem 2** and their simulation results using COMSOL, where we use "Ana." and "Sim." to abbreviate "Analytical" and "Simulation", respectively, and this notation is also used throughout the rest of this paper. We set the parameters: $C_{A_0} = C_{B_0} = 1.5$mol/m^3 in **Theorem 1**, $C_{A_0} = 3$mol/m^3 in **Theorem 2**, $\mu = 2$, $\sigma^2 = 0.25$, $D = 10^{-8}$m^2/s, $k = 400$m^3/(mol·s), $T_{\text{ON}} = 2$s. The simulation points are plotted using the outlet of a straight microfluidic channel with rectangular-shaped cross section, $h = 10\mu$m and $w = 20\mu$m, where the species A and B are both injected with the same velocity $v_{\text{eff}} = 0.2$cm/s. In Fig. 4, it clearly demonstrates a close match between the analytical curves and the simulation points with different channel length L. In Fig. 5, we observe that both approximation methods capture the residual concentration variation of A after reaction $A+B \rightarrow AB$. When C_A approaches to zero, the curve using the second approximation method is smoother than that using the first approximation method due to the consideration of diffusion effect.
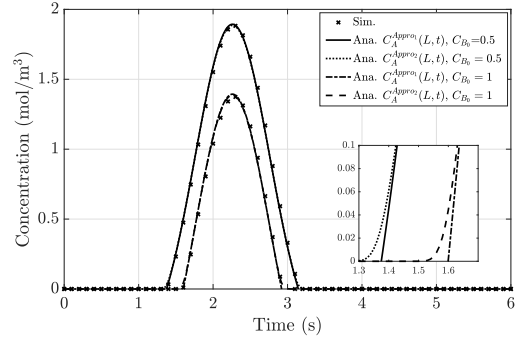
IV. MICROFLUIDIC MC TRANSMITTER ANALYSIS AND DESIGN OPTIMIZATION

In this section, we first analyse the Y Junction and three reaction channels, and then we provide the microfluidic transmitter design in terms of the optimal design of the Reaction II channel length and the restricted time gap between two consecutive input bits, which enable us to control the maximum concentration of a generated pulse and ensure a continuous transmission of non-distorted pulses, respectively.

A. Microfluidic MC Transmitter Analysis

1) Y Junction: The fluid flow containing input reactant X with concentration

$$C_X^{\text{II}}(x, t) = C_{X_0}^{\text{II}}[u(t) - u(t - T_{\text{ON}})] \tag{24}$$
$$\text{and } C_X^{\text{III}}(x, t) = C_{X_0}^{\text{III}}[u(t) - u(t - T_{\text{ON}})] \tag{25}$$

is injected into Inlet II and Inlet III using syringe pumps, where $u(t)$ is the Heaviside step function. The reactant S_y with concentration $C_{S_{y_0}}^{\text{I}}$ and reactant S_p with concentration $C_{S_{p_0}}^{\text{VI}}$ are continuously injected into Inlet I and Inlet IV, respectively. We let the inlets of a Y Junction as the location origin ($x = 0$) and let the time that species are injected at Y Junction inlets as the time origin ($t = 0$). For Y Junction I, the outlet concentration of species X can be expressed using (13) in **Theorem 1** with $C_{B_0} = 0$ and a substitution of $C_{X_0}^{\text{II}}$ for C_{A_0}. However, the complicated form of (13) will make Reaction I channel intractable since the outlet concentration of species X at Y Junction I is an initial boundary condition for the convection-diffusion-reaction equation describing Reaction I channel. Taking into account that the Y Junction length is shorter than the Reaction I channel length, for simplicity, we assume the outlet concentration of species X is only a time shift of its injected concentration due to the travelling of Y Junction I, that is

$$C_X(L_Y, t) \approx C_{X_0}^{\text{II}}[u(t - t_Y) - u(t - T_{\text{ON}} - t_Y)], \tag{26}$$

where $t_Y = \frac{\sqrt{2}L_Y}{v_{\text{eff}}}$ is the travelling time of a Y Junction (L_Y is marked in Fig. 3). Apparently, the above analysis can also be applied to Y junction II.
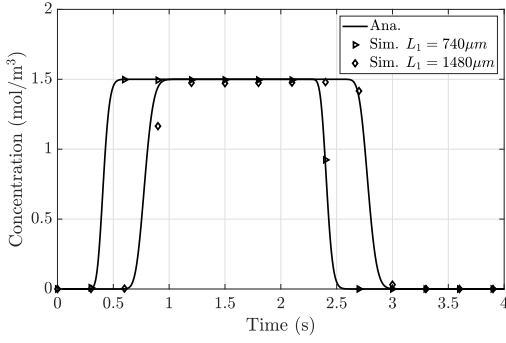
Fig. 6. The concentration of species Y at Reaction I channel outlet with Y Junction I.

2) Straight Reaction I Channel: The outflow of Y junction I enters Reaction I channel to activate Reaction I in (1). The simultaneous flush of independent X and S_y leads to a concentration dilution, which can be treated as diluting species X using S_y or diluting species S_y using X. Hence, with the assumption of (26), the concentration of species X and S_y at the inlet of Reaction I channel become $\frac{1}{2}C_X(L_Y, t)$ and $\frac{1}{2}C^I_{S_{y_0}}$, respectively. Based on this, the outlet concentration of species Y can be expressed using (14) in **Theorem 1** by substituting C_{A_0} and C_{B_0} with $C^{II}_{X_0}$ and $C^I_{S_{y_0}}$, that is

$$C_Y(L_Y + L_1, t) \approx \frac{1}{2}C_{AB}(L_1, t - t_Y). \quad (27)$$

Fig. 6 plots the concentration of species Y at Reaction I channel outlet with Y Junction I. We set the parameters: $C^{II}_{X_0} = C^I_{S_{y_0}} = 3\text{mol/m}^3$, $D = 10^{-8}\text{m}^2/\text{s}$, $k = 400\text{m}^3/(\text{mol}\cdot\text{s})$, $T_{\text{ON}} = 2\text{s}$, $v_{\text{eff}} = 0.2\text{cm/s}$, $L_Y = 60\mu\text{m}$, $h = 10\mu\text{m}$ and $w = 10\mu\text{m}$. It is evident that simulation points are in agreement with theoretical analysis in (27) under different L_1, which validates the analysis of straight Reaction I channel.

3) Serpentine Reaction II Channel: The analysis of straight Reaction I channel can also be applied to serpentine Reaction II channel, which yields

$$C_P(L_Y + L_1, t) \approx \frac{1}{2}C_{AB}(L_2, t - t_Y). \quad (28)$$

This can be explained by the following reasons: 1) although turning corners in the serpentine channel usually cause different laminar flows propagating different distances, we can approximate outlet concentrations of the serpentine channel as those of a straight channel with equivalent length when fluids are in low Reynolds number with very small side length tube, and 2) the form of the convection-diffusion-reaction equation and its initial boundary conditions stills hold with only a substitution of $C_P(x, t)$, $C^{IV}_{S_{P_0}}$, and $C^{III}_{X_0}$ for $C_Y(x, t)$, $C^I_{S_{y_0}}$, and $C^{II}_{X_0}$, respectively.

4) Straight Reaction III Channel: The generated species Y and P mix with each other at a conjunction with length L_C and leads to a concentration dilution before flowing to the Reaction III channel. Therefore, at the inlet of straight Reaction III channel, the concentrations of species Y and P
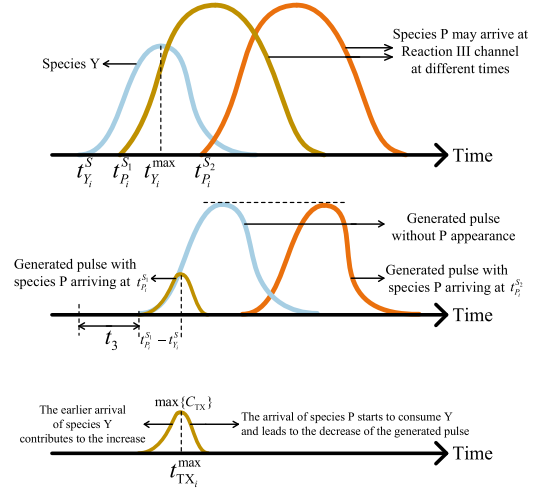

Fig. 7. The generated pulses with different arriving time of species P at Reaction III channel. t_3 is the travelling time over Reaction III channel.

are

$$C_Y(L_Y + L_1 + L_C, t) \approx \frac{1}{4}C_{AB}(L_1, t - t_Y - t_C), \quad (29)$$

$$\text{and } C_P(L_Y + L_1 + L_C, t) \approx \frac{1}{4}C_{AB}(L_2, t - t_Y - t_C), \quad (30)$$

where $t_C = \frac{L_C}{v_{\text{eff}}}$ is the travelling time of the conjunction. When both species Y and P appear in Reaction III channel, Reaction III in (3) is activated, and the corresponding convection-diffusion-reaction equations can be constructed as (10) and (11). Unfortunately, it is foreseeable that deriving the spatial-temporal concentration distribution of species Y, exactly the distribution of the generated pulse, is intractable, since the initial condition with the form of C_{AB} in (14) is mathematically not solvable in closed-form. However, it is possible to obtain the maximum concentration of the generated pulse, which will be presented in the next subsection.

B. Microfluidic MC Transmitter Design

1) Optimal Design of the Reaction II Channel Length: As stated earlier, the maximum concentration of a generated pulse, denoted as $\max\{C_{\text{TX}}\}$, can be obtained, although the convection-diffusion-reaction equation describing Reaction III channel cannot be theoretically solved. In fact, there are many factors affecting $\max\{C_{\text{TX}}\}$, such as the rate constant k and reaction channel lengths L_1, L_2, and L_3. However, if we assume that the rate constant k and reaction channel lengths collectively ensure that reactants are fully converted into a product in each reaction, the Reaction II channel length L_2 will be the only parameter affecting $\max\{C_{\text{TX}}\}$.

At the transmitter, the design of channel length $L_2 > L_1$ allows species Y to first enter the Reaction III channel with a result of the concentration increase of a generated pulse, while the late arrival of species P prevents this increase, and leads to a decrease of the generated pulse, as Y will be immediately depleted by P as soon as P appears in Reaction III channel (shown in Fig. 7). Let us denote the arriving and leaving time of a general species A at Reaction III channel inlet as $t^S_{A_i}$ and

(a) 0 delay line, $\max\{C_{\text{TX}}\}$ $= \frac{1}{3}C_Y(L_Y + L_1 + L_C, t)$.

(b) 1 delay line, $\max\{C_{\text{TX}}\}$ $= \frac{2}{3}C_Y(L_Y + L_1 + L_C, t)$.

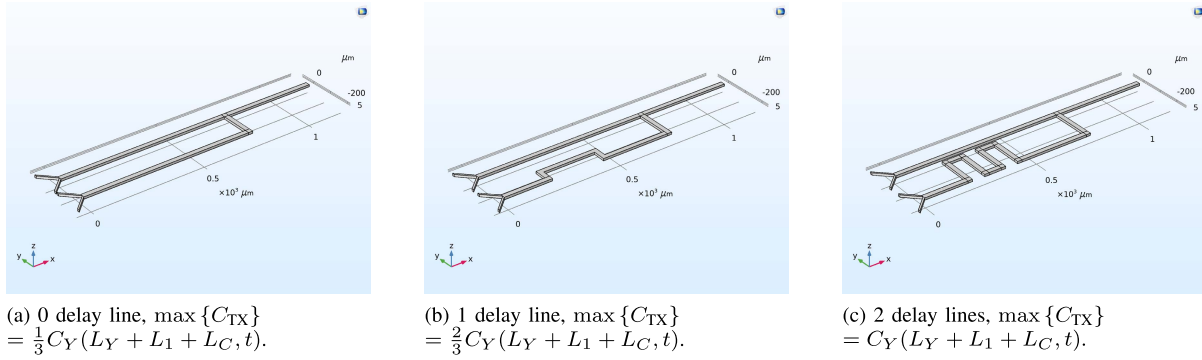(c) 2 delay lines, $\max\{C_{\text{TX}}\}$ $= C_Y(L_Y + L_1 + L_C, t)$.

Fig. 8. Optimized transmitter implementations with different numbers of delay lines in COMSOL.

$t^E_{A_i}$ for the ith input bit, and the time that species A reaches its maximum concentration at Reaction III channel inlet as $t^{\max}_{A_i}$. There are two situations that lead to different $\max\{C_{\text{TX}}\}$.

- If $t^S_{P_i} < t^{\max}_{Y_i}$, the generated pulse will be consumed by P before reaching $\max\{C_Y(L_Y + L_1 + L_C, t)\}$, causing $\max\{C_{\text{TX}}\} < \max\{C_Y(L_Y + L_1 + L_C, t)\}$.
- If $t^S_{P_i} > t^{\max}_{Y_i}$, the generated pulse will reach $\max\{C_Y(L_Y + L_1 + L_C, t)\}$, where the reaction between Y and P only influences the tail shape of the generated pulse.

Therefore, we conclude $\max\{C_{\text{TX}}\} = \zeta C_Y(L_Y + L_1 + L_C, t)$ with $\zeta \in [0, 1]$. Meanwhile, the arriving time of species P is determined by the length of Reaction II channel L_2. As such, we can flexibly control $\max\{C_{\text{TX}}\}$ by choosing different L_2. Based on this, we propose a step-by-step L_2 optimization flow as follows:

Initialization: Given L_1, ζ, and initial concentrations $C^I_{S_{y_0}}$, $C^{II}_{X_0}$, $C^{III}_{X_0}$, and $C^{IV}_{S_{p_0}}$.

Step 1:

1) Search for the time $t^{\max}_{Y_i}$ to satisfy

$$0 \leq \frac{\mathrm{d}C_Y(L_Y + L_1 + L_C, t)}{\mathrm{d}t} \leq \delta, \ t \leq t^{\max}_{Y_i}, \quad (31)$$

$$-\delta \leq \frac{\mathrm{d}C_Y(L_Y + L_1 + L_C, t)}{\mathrm{d}t} \leq 0, \ t > t^{\max}_{Y_i}, \quad (32)$$

where $C_Y(L_Y + L_1 + L_C, t)$ is given in (29). It is noted that we introduce a small variable δ to numerically find $t^{\max}_{Y_i}$, as it is difficult to analytically solve $\frac{\mathrm{d}C_Y(L_Y+L_1+L_C,t)}{\mathrm{d}t} = 0$.

2) Calculate the maximum concentration of a generated pulse that $\max\{C_{\text{TX}}\} = \zeta C_Y(L_Y + L_1 + L_C, t^{\max}_{Y_i})$.

3) Calculate the time $t^{\max}_{\text{TX}_i}$ to satisfy $C_Y(L_Y + L_1 + L_C, t^{\max}_{\text{TX}_i}) = \max\{C_{\text{TX}}\}$.

4) Calculate the Reaction II channel length L_2 via searching for

$$C_P(L_Y + L_1 + L_C, t^{\max}_{\text{TX}_i}) \geq \epsilon, \ x \leq L_2, \quad (33)$$

$$C_P(L_Y + L_1 + L_C, t^{\max}_{\text{TX}_i}) < \epsilon, \ x > L_2, \quad (34)$$

where $C_P(L_Y + L_1 + L_C, t)$ is given in (30). Similar to δ, ϵ is introduced here to numerically find L_2.

To examine the proposed L_2 optimization flow, we implement three designs with different numbers of delay lines in

TABLE I
THE PARAMETERS OF THE PROPOSED MICROFLUIDIC TRANSMITTER

Channel	Length(μm)	Width(μm)	Depth(μm)
Y Junction	$L_Y = 60$	10	10
Conjunction	$L_C = 20$	20	10
Reaction I Channel	$L_1 = 740$	20	10
Reaction III Channel	$L_3 = 400$	20	10

COMSOL to achieve different $\max\{C_{\text{TX}}\}$. The implementation is shown in Fig. 8 and geometric parameters are listed in Table I and Table II. Other parameters are set following: $C^I_{S_{y_0}} = C^{II}_{X_0} = 3\text{mol/m}^3$, $C^{III}_{X_0} = C^{IV}_{S_{p_0}} = 4\text{mol/m}^3$, $D = 10^{-8}\text{m}^2/\text{s}$, $k = 400\text{m}^3/(\text{mol·s})$, $T_{\text{ON}} = 2\text{s}$, $v_{\text{eff}} = 0.2\text{cm/s}$. Here, we modify $\max\{C_Y(L_Y + L_1 + L_C, t)\}$ from 0.75 to 0.7498. As shown in Fig. 6, when $L_1 = 740\mu$m, $C_Y(L_Y + L_1, t)$ rapidly reaches 1.4995 at 0.55s and then increases very slowly to the maximum concentration 1.5 at 0.9511s. It takes 0.4s to reach the maximum concentration from 1.4995, while the concentration increase is less than 0.001. In order to generate a pulse that both two sides of the maximum concentration show a distinct increase or decrease, we modify $\max\{C_Y(L_Y + L_1, t)\}$ and $t^{\max}_{Y_i}$ as 1.4995 and 0.55s, respectively, thus $\max\{C_Y(L_Y + L_1 + L_C, t)\} = \frac{1}{2}\max\{C_Y(L_Y + L_1, t)\} = 0.7498$.

In Fig. 9, we plot the concentrations of generated pulses for implementations in Fig. 8. As expected, the output pulses are generated successfully during T_{ON}, and all the maximum concentrations of the pulses reach their corresponding analytical values (marked in black dash-dot lines). It is also seen that the longer the Reaction II channel is, the wider the generated pulse, because of the longer time given to reach a higher maximum concentration. However, we remark that there is a trade-off between the maximum concentration and the pulse width, as a wider generated pulse is more likely to cause the inter-symbol-interference (ISI). These observations reveal the dependency of the maximum concentration of a generated pulse on the Reaction II channel length L_2, show how the predefined shaping of the pulse can be controlled, and highlight the importance of deriving theoretical signal responses in design stage. Knowing that different concentration levels can represent various symbols, the results also demonstrate the capability of optimization flow in implementing higher-order *CSK* to enhance the data rate. In addition, the black dash

TABLE II
THE PARAMETERS OF SERPENTINE REACTION II CHANNEL IN FIG. 8

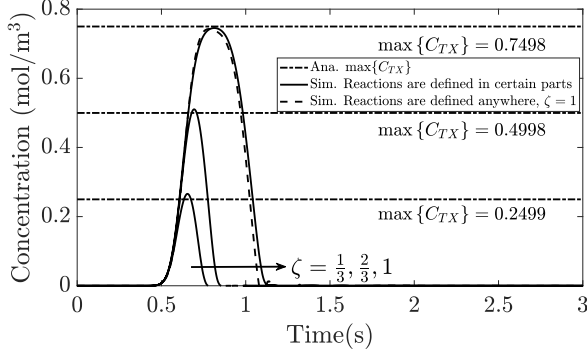| Channel	$L_2(\mu m)$	$L_{21}(\mu m)$	$L_{22}(\mu m)$	$L_{23}(\mu m)$	$L_s(\mu m)$	$H_s(\mu m)$	ζ	δ	ϵ
0 delay line	887	/	/	137	/	/	1/3	0.13	10^{-1}
1 delay line	1019	200	300	157	250	56	2/3	0.13	3×10^{-2}
2 delay lines	1516	200	325	177	75	147.25	1	0.13	10^{-3}

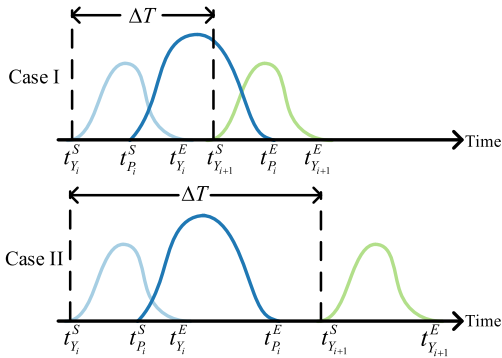Fig. 9. The concentrations of generated pulses for different transmitter implementations.

Fig. 10. The concentrations of species Y and P at Reaction III channel inlet with different time gaps.

line represents the simulation results that the three chemical reactions in (1)-(3) are defined in all channels in Fig. 8(c). We can see that the transmitter output is almost the same with the results that reactions are defined in certain parts. The reason is that the selected channel lengths, mean velocity, and rate constant can jointly allow for completing reactions fast enough before leaving defined regions.

2) Optimal Design of the Restricted Time Gap: The design that the Reaction II channel is longer than the Reaction I channel ($L_2 > L_1$) is also likely to cause distorted pulses if the time gap ΔT between two consecutive input bits is not chosen appropriately. Assuming that species Y generated by the $(i + 1)$th input bit arrives earlier than the leaving time of species P generated by the ith input bit at Reaction III channel inlet, Y will be immediately consumed according to Reaction III when they simultaneously enter the Reaction III channel so that the maximum concentration of the generated pulse for the $(i + 1)$th input bit is distorted and less than $\max\{C_{TX}\}$. To prevent this, the time gap ΔT should be restricted.

Recall that the arriving and leaving time of a general species A at Reaction III channel inlet are denoted as $t_{A_i}^S$ and $t_{A_i}^E$ for the ith input bit. As shown in Fig. 10, species Y generated by the $(i+1)$th input bit can appear earlier in Case I or later in Case II than species P generated by the ith input bit via adjusting ΔT. In Case I, the earlier arriving of Y makes itself react with the tail of P, thus breaking the principle that Y should increase to $\max\{C_{TX}\}$ and then drop to zero. To avoid this, ΔT needs to satisfy

$$\Delta T \geq t_{P_i}^E - t_{Y_i}^S, \tag{35}$$

where $t_{Y_i}^S$ and $t_{P_i}^E$ can be numerically solved by

$$
\begin{aligned}
C_Y(L_Y + L_1 + L_C, t) &\leq \tau, & t \leq t_{Y_i}^S, \\
C_Y(L_Y + L_1 + L_C, t) &> \tau, & t > t_{Y_i}^S;
\end{aligned}
\tag{36}
$$

$$
\begin{aligned}
C_P(L_Y + L_1 + L_C, t) &\geq \tau, & t \leq t_{P_i}^E, \\
C_P(L_Y + L_1 + L_C, t) &< \tau, & t > t_{P_i}^E.
\end{aligned}
\tag{37}
$$

Here, τ is a small variable to find $t_{Y_i}^S$ and $t_{P_i}^E$ that $C_Y(L_Y + L_1 + L_C, t_{Y_i}^S) = 0$ and $C_P(L_Y + L_1 + L_C, t_{P_i}^E) = 0$, respectively.

In Fig. 11, we plot the concentrations of species Y and P at Reaction III channel inlet and the generated pulses with different ΔT. We use the parameters for Fig. 8 (c) and $\tau = 10^{-3}$. We numerically solve (36), (37) and obtain $\Delta T \geq 2.75$s. Fig. 11 (c) shows that the second pulse is distorted compared with the first pulse because $\Delta T = 2.3$s leading to the earlier arriving of species Y generated by the 2nd input bit, and thus a twice consumption of Y, being first consumed by the tail of P generated by the 1st input bit and then by the arriving of P generated by the 2nd input bit. On the contrary, Fig. 11 (d) illustrates a generation of two non-distorted and identical-shaped pulses with a satisfied ΔT.

V. MICROFLUIDIC MC RECEIVER ANALYSIS AND DESIGN

In this section, we analyse the T Junction and two reaction channels, and then provide some guidelines on how to design a microfluidic MC receiver.

A. Microfluidic MC Receiver Analysis

1) T Junction: After information propagation, the transmitted molecules Y from the microfluidic transmitter propagate to enter the receiver through Inlet V. Here, we set the location of Inlet V as the position origin and the time that species Y flows into Inlet V as the time origin. Since the transmitted pulse cannot be theoretically derived, we use a Gaussian concentration distribution with mean μ and variance σ^2 to represent the received pulse, which is
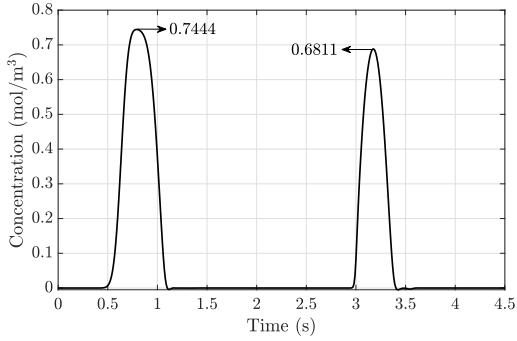
$$C_Y(0, t) = \frac{C_{Y_0}^V}{\sqrt{2\pi\sigma^2}} e^{-\frac{(t-\mu)^2}{2\sigma^2}}. \tag{38}$$
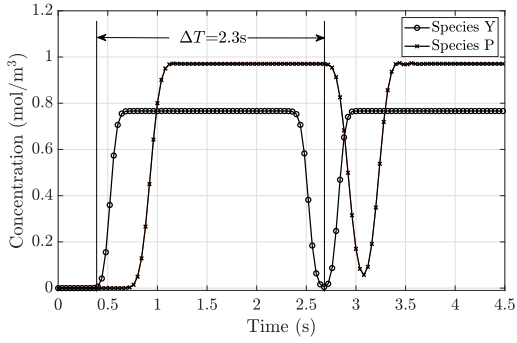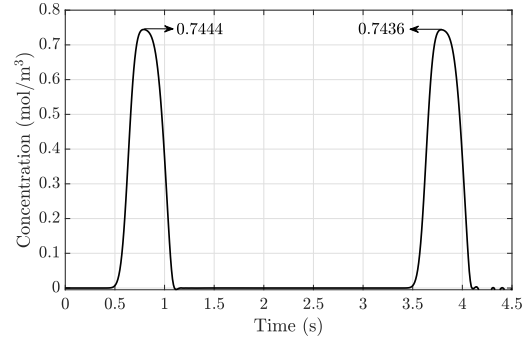
(a) The durations of two consecutive input bits are $[0.1, 2.1]$ and $[2.4, 4.4]$
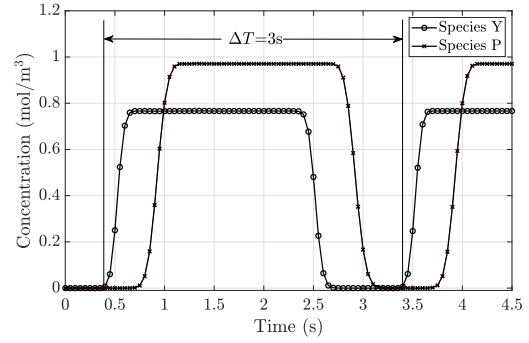
(b) The durations of two consecutive input bits are $[0.1, 2.1]$ and $[3.1, 5.1]$.

(c) The generated pulses of (a).

(d) The generated pulses of (b).

Fig. 11. The concentrations of species Y and P at Reaction III channel inlet and their generated pulses with different ΔT.

Although a Gaussian concentration profile is considered, it is noted that the methodology to derive **Theorem 2** and analyse the receiver performance can also deal with other concentration profiles.

As the length of one T junction branch L_T is much shorter than that of the following reaction channel, and no reaction happens in a T junction, we further assume the concentration of species Y at T junction I outlet as

$$C_Y(L_T + L_C, t) \approx \frac{1}{2}C_Y(0, t - t_T), \qquad (39)$$

where the $\frac{1}{2}$ describes the dilution of species Y by species ThL that is continuously injected into Inlet VI particularly with concentration C_{ThL}^{VI}, and $t_T = \frac{L_T}{v_{eff}} + \frac{L_C}{2v_{eff}}$ is the travelling time over T junction I particularly with a doubled velocity through L_C due to the fluxes from Inlet V and Inlet VI. Similarly, the outlet concentration of species ThL is assumed as

$$C_{ThL}(L_T + L_C, t) \approx \frac{1}{2}C_{ThL}^{VI}, \quad t \geq t_T. \qquad (40)$$

2) Straight Reaction IV Channel: The outflow of T junction I flows through the Reaction IV channel with length L_4 to proceed Reaction IV (the thresholding reaction) in (4), where the portion of species Y, whose concentration below $\frac{1}{2}C_{ThL}^{IV}$, is depleted by reactant ThL. With assumptions of (39) and (40), the concentration of species Y at Reaction IV channel outlet can be expressed using (18) or (19) in **Theorem 2** by

substituting C_{A_0} and C_{B_0} with $C_{Y_0}^{V}$ and C_{ThL}^{VI}, which yields

$$\begin{aligned} C_Y&(L_T + L_C + L_4, t) \\ &\approx \frac{1}{2}C_A^{Appro_1}(L_4, t - t_T) \text{ or } \frac{1}{2}C_A^{Appro_2}(L_4, t - t_T). \end{aligned} \qquad (41)$$

3) Straight Reaction V Channel: After Reaction IV, the remaining species Y flows into the Reaction V channel and catalyses the conversion of species Amp into output species O, where Amp is continuously infused with constant concentration C_{Amp}^{VII} into Inlet VII. As a catalyst, species Y does not react with species Amp, and the produced quantity of species O equals the reacting concentration of Amp according to their stoichiometric relation. Considering the dilution at T junction II, the reacting concentration of Amp is diluted to one third of its injected concentration by flows injected at Inlet V and Inlet VI. Based on this and ignoring the diffusion effect in Reaction V channel, the demodulated signal containing species O can be approximated as

$$\begin{aligned} C_O&(t) \\ &= \begin{cases} \frac{1}{3}C_{Amp}^{VII}, & C_Y(L_T + 2L_C + L_4 + L_5, t - \frac{L_C + L_5}{3v_{eff}}) \geq 0, \\ 0, & \text{otherwise,} \end{cases} \end{aligned}$$

$$(42)$$

It is noted that without the broadening of diffusion [40], the pulse width of (42) is exactly a lower bound of the rectangular width.

TABLE III

THE PARAMETERS OF THE PROPOSED MICROFLUIDIC RECEIVER

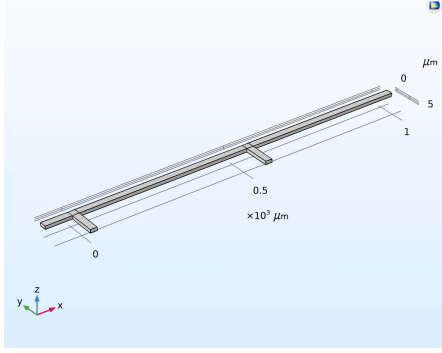| Channel	Length(μm)	Width(μm)	Depth(μm)
T Junction	$L_T = 80$	20	10
Conjunction	$L_C = 20$	20	10
Reaction IV Channel	$L_4 = 520$	20	10
Reaction V Channel	$L_5 = 470$	20	10

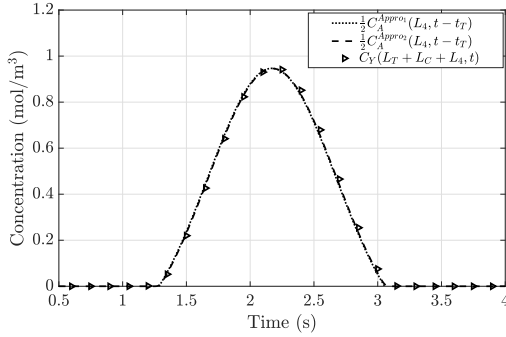Fig. 12. The proposed microfluidic receiver implementation in COMSOL.

Fig. 13. The concentration of species Y at Reaction IV channel outlet with T Junction I.

4) Simulation Results: To examine the microfluidic receiver analysis, we implement the receiver design in COM-SOL (shown in Fig. 12) with geometric parameters listed in Table III.

We set the parameters: $C_{Y_0}^V = 3\text{mol/m}^3$, $\mu = 2$, $\sigma^2 = 0.25$, $k = 400\text{m}^3/(\text{mol·s})$, $D = 10^{-8}\text{m}^2/\text{s}$, and $v_{\text{eff}} = 0.2\text{cm/s}$.

Fig. 13 compares the concentration of species Y at Reaction IV channel outlet with the two approximations in (41). We observe that the two approximations can still capture the simulation output. However, please note that the velocity in the first conjunction and the Reaction IV channel becomes the twice of the injected velocity because the the conjunction and the Reaction IV channel handle two fluxes from Inlet V and Inlet VI while have the same cross-sectional area with these inlets.

Fig. 14 demonstrates the significant role of C_{ThL}^{VI} on the width of the demodulated signal $C_O(t)$. As C_{ThL}^{VI} increases, the width of the demodulated signal decreases. If $C_{ThL}^{VI} > \max\{C_Y(0,t)\}$, we expect that there is no residual Y in Reaction V channel, so that species O cannot be produced. Fig. 15 plots the concentrations of species O at Reaction V channel outlet with different C_{Amp}^{VII}. As expected, the outlet
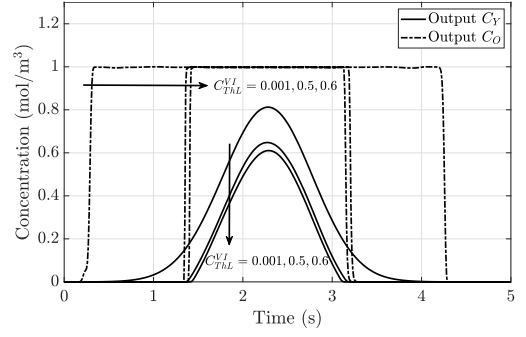

Fig. 14. The concentrations of species Y and O at Reaction V channel outlet with different C_{ThL}^{VI}, where the concentration of species O is normalized to 1mol/m^3.
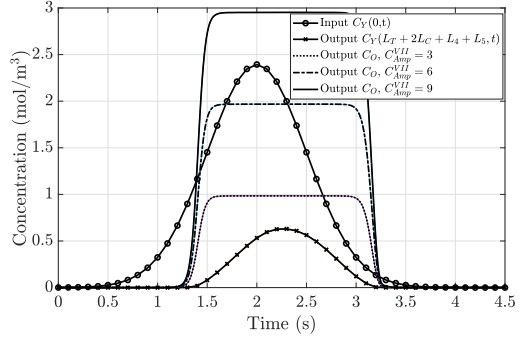

Fig. 15. The outlet concentrations of species O at Reaction V channel with different C_{Amp}^{VII}.
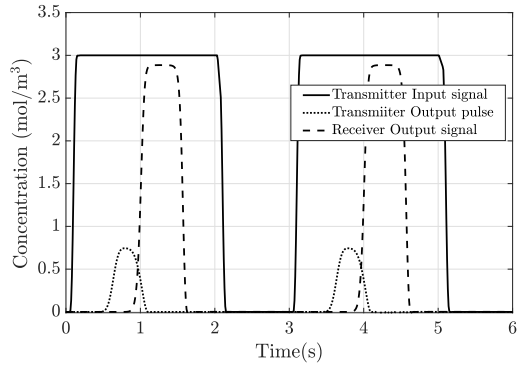
Fig. 16. The transmitter input signals, transmitter output pulses, and receiver output signals for the basic end-to-end MC implementation.

concentration of species O varies with C_{Amp}^{VII}, and approximately equals $\frac{1}{3}C_{Amp}^{VII}$, which reveals that it is possible to reach any level C_O via adjusting C_{Amp}^{VII}.

B. Microfluidic MC Receiver Design

Based on the simulation results in Fig. 14 and 15, we conclude two receiver design guidelines. First, the results in Fig. 14 reveal that the demodulated signal width is dependent on C_{ThL}^{VI}, and C_{ThL}^{VI} cannot exceed the maximum concentration of a received pulse, which in turn highlights the necessity and importance to study the maximum concentration control of a generated pulse in Sec. IV-B.1. Second, the results in Fig. 15 present the relation between C_{Amp}^{VII} and C_O follows

$C_O = \frac{1}{3}C_{Amp}^{\text{VII}}$. This insight is helpful in concentration detection. If concentration is detected through fluorescence, the relation $C_O = \frac{1}{3}C_{Amp}^{\text{VII}}$ enables us to determine how much C_{Amp}^{VII} should be injected to ensure fluorescent species O to be captured by a microscopy.

VI. AN END-TO-END MICROFLUIDIC MC IMPLEMENTATION

In this section, we combine the microfluidic transmitter with the receiver as proposed in Fig. 3 to form a basic end-to-end MC system, where the transmitter and the receiver share the same design parameters as implementations in Fig. 11(b) and Fig. 12, and the propagation channel is a straight convection-diffusion channel with length 1000μm. Considering the reacting concentration of species Amp is diluted to one fourth of its injected concentration C_{Amp}^{VII} by flows from Y Junction I outlet, Y Junction II outlet, and Inlet VI, we set $C_{Amp}^{\text{VII}} = 12$mol/m^3 for the purpose of restoring the output concentration level to input concentration of species X injected at Inlet II ($C_{X_0}^{\text{II}} = 3$mol/m^3).

Fig. 16 plots the transmitter input signals, transmitter output pulses, and receiver output signals. It is clear that two consecutive rectangular signals are successfully demodulated, and this result demonstrates the validity of the end-to-end MC system. Moreover, we observe that although the concentrations of transmitter output pulses are much lower than concentrations of transmitter input signals due to two dilutions occurred on Y Junction output and the conjunction between Reaction I/II channel and Reaction III channel, the concentrations of receiver output signals can approximately restore to the same concentration level of input signal via adjusting C_{Amp}^{VII}.

After validating the microfluidic design in COMSOL, the device can then be fabricated in polydimethylsiloxane (PDMS) via soft lithography [41], [42]. We envision that a syringe, connected with a species reservoir and a computer, is placed next to each inlet, and its injection is controlled by this computer via digital commands. To detect the output concentration, we can use optical based techniques [43].

VII. CONCLUSION

In this paper, we first optimized our previous transmitter design. Specifically, we proposed a reaction channel length optimization framework to control the maximum concentration of output pulse at the transmitter, and then derived a time gap constraint between two consecutive input bits to ensure a continuous transmission of non-distorted and identical-shaped pulses upon consecutive digital inputs. We then proposed a microfluidic receiver design based on a thresholding reaction and an amplifying reaction to realize a function of demodulating a received signal into a rectangular output signal. Both the proposed designs were based on microfluidic systems with standard and reproducible components, and these microfluidic components were analytically characterized to reveal the dependence of the generated pulse and the demodulated signal on design parameters. Finally, we implemented an end-to-end microfluidic MC system through connecting the transmitter with the receiver, and simulation results performed in COMSOL Multiphysics demonstrated successfully pulse generation and signal demodulation, thus effectiveness of the proposed designs. Notably, our proposed microfluidic transceiver will act as fundamental building blocks in the design of future micro/nanoscale MC systems. More importantly, the methodology presented in this paper will inspire the design of additional MC blocks inspired by biochemical processes and based on microfluidic systems.

APPENDIX A
PROOF OF THEOREM 1

To solve the spatial-temporal concentration distributions of species A and AB, we first define some initial boundary conditions. Species A and B are injected at the inlet of a straight microfluidic channel $x = 0$, the first initial boundary condition is

$$
\begin{aligned}
C_A(0,t) &= \min\{C_{A_0}, C_{B_0}\} = C_0, \quad 0 \le t \le T_{\text{ON}} \\
&= C_0[u(t) - u(t - T_{\text{ON}})].
\end{aligned} \tag{43}
$$

Here, we must be careful that $C_A(0,t)$ may not equal its injected concentration. This is because the one-to-one stoichiometric relation between species A and B in $A + B \rightarrow AB$ determines that either the reacting concentration of species A or B equals the smaller supplied concentration, $i.e.$, $\min\{C_{A_0}, C_{B_0}\}$. At $t = 0$, the concentration of species A in any positions is zero, thus the second initial boundary condition being

$$
C_A(x,0) = 0, \quad x \ge 0. \tag{44}
$$

As the concentration change over locations far away from the source equals zero, the third boundary condition is

$$
\frac{\partial C_A(\infty,t)}{\partial x} = 0, \quad t \ge 0. \tag{45}
$$

The concentration distribution can be obtained by taking the Laplace transform of (10), (43), and (45) using

$$
\widetilde{C_A}(x,s) = \int_0^\infty e^{-st} C_A(x,t)\,\mathrm{d}t. \tag{46}
$$

The Laplace transform of (10) satisfying (44) is

$$
D_{\text{eff}}\frac{\partial^2 \widetilde{C_A}(x,s)}{\partial x^2} - v_{\text{eff}}\frac{\partial \widetilde{C_A}(x,s)}{\partial x} = (s + kC_0)\,\widetilde{C_A}(x,s). \tag{47}
$$

The Laplace transforms of (43) and (45) can be expressed

$$
\widetilde{C_A}(0,s) = \frac{C_0}{s}(1 - e^{-T_{\text{ON}}s}), \tag{48}
$$

$$
\text{and } \frac{\partial \widetilde{C_A}(\infty,s)}{\partial x} = 0. \tag{49}
$$

Combining (47), (48), and (49), we derive

$$
\begin{aligned}
\widetilde{C_A}(x,s) =\ & \frac{C_0(1 - e^{-T_{\text{ON}}s})}{s} \\
& \exp\left[\frac{v_{\text{eff}}x}{2D_{\text{eff}}} - x\sqrt{\frac{v_{\text{eff}}^2}{4D_{\text{eff}}^2} + \frac{s + kC_0}{D_{\text{eff}}}}\right].
\end{aligned} \tag{50}
$$

Taking the inverse Laplace transform of (50), we derive

$$C_A(x,t) = \begin{cases} g(x,t), & 0 \leq t \leq T_{\text{ON}} \\ g(x,t) - g(x, t - T_{\text{ON}}), & t > T_{\text{ON}}, \end{cases} \quad (51)$$

where

$$g(x,t) = \frac{C_0}{2} \left\{ \exp\left[\frac{(v_{\text{eff}} - \alpha)x}{2D_{\text{eff}}} \right] \text{erfc}\left[\frac{x - \alpha t}{2\sqrt{D_{\text{eff}}t}} \right] \right.$$
$$\left. + \exp\left[\frac{(v_{\text{eff}} + \alpha)x}{2D_{\text{eff}}} \right] \text{erfc}\left[\frac{x + \alpha t}{2\sqrt{D_{\text{eff}}t}} \right] \right\} \quad (52)$$

with $\alpha = \sqrt{v_{\text{eff}}^2 + 4kC_0 D_{\text{eff}}}$.

To derive the concentration of species AB, we combine (10) and (11) as

$$D_{\text{eff}} \frac{\partial^2 C_s(x,t)}{\partial x^2} - v_{\text{eff}} \frac{\partial C_s(x,t)}{\partial x} = \frac{\partial C_s(x,t)}{\partial t}, \quad (53)$$

where $C_s(x,t) = C_A(x,t) + C_{AB}(x,t)$. Interestingly, this equation is the convection-diffusion equation for the total concentration distribution of molecule A and AB. The sum concentration of A and AB follows the three boundary conditions

$$C_s(0,t) = C_0, \quad 0 \leq t \leq T_{\text{ON}}, \quad (54)$$
$$C_s(x,0) = 0, \quad x \geq 0, \quad (55)$$
$$\text{and } C_s(\infty,t) = 0, \quad t \geq 0. \quad (56)$$

Following [44, eq. (11)], we can derive the molecular concentration as

$$C_s(x,t) = \begin{cases} h(x,t), & 0 \leq t \leq T_{\text{ON}} \\ h(x,t) - h(x, t - T_{\text{ON}}), & t > T_{\text{ON}}, \end{cases} \quad (57)$$

where $h(x,t) = \frac{C_0}{2} \left[\text{erfc}\left(\frac{x - v_{\text{eff}}t}{2\sqrt{D_{\text{eff}}t}} \right) + e^{\frac{v_{\text{eff}}x}{D_{\text{eff}}}} \text{erfc}\left(\frac{x + v_{\text{eff}}t}{2\sqrt{D_{\text{eff}}t}} \right) \right]$.
Taking the deduction of $C_A(x,t)$ in (51) from $C_s(x,t)$, we derive the concentration of AB as

$$C_{AB}(x,t)$$
$$= \begin{cases} h(x,t) - g(x,t), & \\ & 0 \leq t \leq T_{\text{ON}}, \\ [h(x,t) - g(x,t)] - [h(x, t - T_{\text{ON}}) - g(x, t - T_{\text{ON}})], & \\ & t > T_{\text{ON}}. \end{cases}$$
$$(58)$$

APPENDIX B
PROOF OF THEOREM 2

Similar to the Proof of **Theorem 1**, we first define initial boundary conditions. On the condition of $C_{B_0} < \max\{C_A(0,t)\}$ and due to the one-to-one stoichiometric relation between A and B, the first initial condition varies with C_{B_0}, and can be expressed as

$$C_A(0,t) = \begin{cases} C_A(0,t), & 0 \leq t < t_1 \\ C_{B_0}, & t_1 \leq t < t_2 \\ C_A(0,t), & t_2 \leq t, \end{cases} \quad (59)$$

where t_1 and t_2 are obtained through solving $C_A(0,t) = C_{B_0}$, and finally $t_1 = \mu - \sqrt{-2\sigma^2 \ln \frac{C_{B_0}\sqrt{2\pi\sigma^2}}{C_{A_0}}}$ and

$t_2 = \mu + \sqrt{-2\sigma^2 \ln \frac{C_{B_0}\sqrt{2\pi\sigma^2}}{C_{A_0}}}$. The second and third initial boundary conditions are the same with (44) and (45), respectively. Next, we introduce two approximation methods to solve (10), where we split the fully coupled convection-diffusion-reaction process into two sequential processes: 1) the reaction process (described by a reaction equation), and 2) the convection/convection-diffusion process (described by a convection/convection-diffusion equation). Under the assumption that $A + B \rightarrow AB$ has been finished as soon as species A and B enter a straight microfluidic channel, we can use the solution of the reaction equation as an initial condition for the convection/convection-diffusion equation.

A. The First Approximation Method

The first method splits (10) into a reaction equation and a convection equation by ignoring the diffusion term. The residual concentration of species A is the portion whose concentration is greater than C_{B_0}, and is expressed as

$$C_A(0,t) - C_{B_0}, \quad t_1 \leq t \leq t_2. \quad (60)$$

The subsequent transport of species A will be only affected by convection. It has also shown in [40] that the convection effect is merely a shift of initial specie profiles in time with velocity v_{eff} and without any change of shape, so the outlet concentration of A at the reaction channel can be expressed as

$$C_A^{\text{Appro}_1}(x,t)$$
$$= \begin{cases} C_A(0, t - \frac{x}{v_{\text{eff}}}) - C_{B_0}, & t_1 + \frac{x}{v_{\text{eff}}} \leq t \leq t_2 + \frac{x}{v_{\text{eff}}}, \\ 0, & \text{otherwise.} \end{cases}$$
$$(61)$$

B. The Second Approximation Method

Different from the first approximation method, the second one takes the diffusion effect into account. The convection-diffusion equation with initial condition in (60) and other boundary conditions can be constructed as

$$\frac{\partial C_A^{\text{Appro}_2}(x,t)}{\partial t} = D_{\text{eff}} \frac{\partial^2 C_A^{\text{Appro}_2}(x,t)}{\partial x^2}$$
$$- v_{\text{eff}} \frac{\partial C_A^{\text{Appro}_2}(x,t)}{\partial x}, \quad (62)$$
$$C_A^{\text{Appro}_2}(0,t) = C_A(0,t) - C_{B_0}, \quad t_1 \leq t \leq t_2, \quad (63)$$
$$C_A^{\text{Appro}_2}(x,0) = 0, \quad x \geq 0, \quad (64)$$
$$\text{and } \frac{\partial C_A^{\text{Appro}_2}(x,t)}{\partial x} \Big|_{x=\infty} = 0, \quad t \geq 0. \quad (65)$$

We take the Laplace transform of (62) with respect to t and obtain

$$D_{\text{eff}} \frac{\partial^2 \widetilde{C_A^{\text{Appro}_2}}(x,s)}{\partial x^2} - v_{\text{eff}} \frac{\partial \widetilde{C_A^{\text{Appro}_2}}(x,s)}{\partial x} - s\widetilde{C_A^{\text{Appro}_2}}(x,s) = 0. \quad (66)$$

The solution of this second order differential equation satisfying the Laplace transforms of (63) and (65) is

$$\widetilde{C_A^{\text{Appro}_2}}(x,s) = l(s)e^{\frac{v_{\text{eff}} - \sqrt{v_{\text{eff}}^2 + 4D_{\text{eff}}s}}{2D_{\text{eff}}}x}, \qquad (67)$$

where $l(s)$ is a coefficient function and is the Laplace transform of (63), which is

$$l(s) = \int_{t_1}^{t_2} [C_A(0,t) - C_{B_0}]e^{-st}\mathrm{d}t$$
$$= C_{A_0}e^{-s\mu}e^{\frac{(\sigma s)^2}{2}}[Q(\frac{t_1 + \sigma^2 s - \mu}{\sigma}) - Q(\frac{t_2 + \sigma^2 s - \mu}{\sigma})]$$
$$- \frac{C_{B_0}}{s}(e^{-st_1} - e^{-st_2}), \qquad (68)$$

where $Q(.)$ is the Q-function.

In order to obtain $C_A^{\text{Appro}_2}(x,t)$, it is necessary to take the inverse Laplace transform of (67). However, due to the complexity of (68), we cannot derive the closed-form expression $\mathcal{L}^{-1}\left\{\widetilde{C_A^{\text{Appro}_2}}(x,s)\right\}$. Hence, we employ the Gil-Pelaez theorem [10], [45]. Considering that the Fourier transform of a probability density function (PDF) is its characteristic function, (67) is firstly converted to Fourier transform $\widetilde{C_A^{\text{Appro}_2}}(x,\omega)$ by substituting $j\omega$ for s, and then we regard $\widetilde{C_A^{\text{Appro}_2}}(x,\omega)$ as the characteristic function of $\mathcal{L}^{-1}\left\{\widetilde{C_A^{\text{Appro}_2}}(x,s)\right\}$. The corresponding cumulative distribution function (CDF) can be given in terms of $\widetilde{C_A^{\text{Appro}_2}}(x,\omega)$ as

$$F(t) = \frac{1}{2} - \frac{1}{\pi}\int_0^\infty \frac{e^{-j\omega t}\overline{\widetilde{C_A^{\text{Appro}_2}}(x,\omega)} - e^{j\omega t}\widetilde{C_A^{\text{Appro}_2}}(x,\omega)}{2j\omega}\mathrm{d}w. \qquad (69)$$

Taking the derivative of $F(t)$, we derive the inverse Laplace transform and obtain the outlet concentration of species A as

$$C_A^{\text{Appro}_2}(x,t) = \frac{1}{2\pi}\int_0^\infty [e^{-j\omega t}\overline{\widetilde{C_A^{\text{Appro}_2}}(x,\omega)} + e^{j\omega t}\widetilde{C_A^{\text{Appro}_2}}(x,\omega)]\mathrm{d}w. \qquad (70)$$

REFERENCES

[1] Y. Deng, M. Pierobon, and A. Nallanathan, "A microfluidic feed forward loop pulse generator for molecular communication," in *Proc. IEEE Global Commun. Conf. (GLOBECOM)*, Dec. 2017, pp. 1–7.

[2] I. F. Akyildiz, F. Brunetti, and C. Blazquez, "Nanonetworks: A new communication paradigm," *Comput. Netw.*, vol. 52, no. 12, pp. 2260–2279, Aug. 2008.

[3] I. F. Akyildiz, M. Pierobon, S. Balasubramaniam, and Y. Koucheryavy, "The Internet of bio-nano things," *IEEE Commun. Mag.*, vol. 53, no. 3, pp. 32–40, Mar. 2015.

[4] N. Farsad, H. B. Yilmaz, A. Eckford, C.-B. Chae, and W. Guo, "A comprehensive survey of recent advancements in molecular communication," *IEEE Commun. Surveys Tuts.*, vol. 18, no. 3, pp. 1887–1919, 3rd Quart., 2016.

[5] H. C. Berg, *Random Walks in Biology*. Princeton, NJ, USA: Princeton Univ. Press, 1993.

[6] H. Bruus, *Theoretical Microfluidics*. London, U.K.: Oxford Univ. Press, 2008.

[7] A. Noel, K. C. Cheung, and R. Schober, "Improving receiver performance of diffusive molecular communication with enzymes," *IEEE Trans. Nanobiosci.*, vol. 13, no. 1, pp. 31–43, Mar. 2014.

[8] Y. Deng, A. Noel, W. Guo, A. Nallanathan, and M. Elkashlan, "3D stochastic geometry model for large-scale molecular communication systems," in *Proc. IEEE Global Commun. Conf. (GLOBECOM)*, Dec. 2016, pp. 1–6.

[9] B. Alberts *et al.*, *Essential Cell Biology*. New York, NY, USA: Garland Science, 2013.

[10] Y. Deng, A. Noel, M. Elkashlan, A. Nallanathan, and K. C. Cheung, "Molecular communication with a reversible adsorption receiver," in *Proc. IEEE Int. Conf. Commun. (ICC)*, May 2016, pp. 1–7.

[11] M. Pierobon and I. F. Akyildiz, "Capacity of a diffusion-based molecular communication system with channel memory and molecular noise," *IEEE Trans. Inf. Theory*, vol. 59, no. 2, pp. 942–954, Feb. 2013.

[12] N. Farsad, Y. Murin, A. Eckford, and A. Goldsmith, "On the capacity of diffusion-based molecular timing channels," in *Proc. IEEE Int. Symp. Inf. Theory (ISIT)*, Jul. 2016, pp. 1023–1027.

[13] M. B. Dissanayake, Y. Deng, A. Nallanathan, M. Elkashlan, and U. Mitra, "Interference mitigation in large-scale multiuser molecular communication," *IEEE Trans. Commun.*, vol. 67, no. 6, pp. 4088–4103, Jun. 2019.

[14] N. Farsad, W. Guo, and A. W. Eckford, "Tabletop molecular communication: Text messages through chemical signals," *PLoS ONE*, vol. 8, no. 12, Dec. 2013, Art. no. e82935.

[15] B.-H. Koo, C. Lee, H. B. Yilmaz, N. Farsad, A. Eckford, and C.-B. Chae, "Molecular MIMO: From theory to prototype," *IEEE J. Sel. Areas Commun.*, vol. 34, no. 3, pp. 600–614, Mar. 2016.

[16] S. Giannoukos, D. T. McGuiness, A. Marshall, J. Smith, and S. Taylor, "A chemical alphabet for macromolecular communications," *Anal. Chem.*, vol. 90, no. 12, pp. 7739–7746, May 2018.

[17] E. De Leo, L. Donvito, L. Galluccio, A. Lombardo, G. Morabito, and L. M. Zanoli, "Communications and switching in microfluidic systems: Pure hydrodynamic control for networking Labs-on-a-Chip," *IEEE Trans. Commun.*, vol. 61, no. 11, pp. 4663–4677, Nov. 2013.

[18] B. Krishnaswamy *et al.*, "Time-elapse communication: Bacterial communication on a microfluidic chip," *IEEE Trans. Commun.*, vol. 61, no. 12, pp. 5139–5151, Dec. 2013.

[19] A. Marcone, M. Pierobon, and M. Magarini, "Parity-check coding based on genetic circuits for engineered molecular communication between biological cells," *IEEE Trans. Commun.*, vol. 66, no. 12, pp. 6221–6236, Dec. 2018.

[20] R. Weiss *et al.*, "Genetic circuit building blocks for cellular computation, communications, and signal processing," *Natural Comput.*, vol. 2, no. 1, pp. 47–84, Mar. 2003.

[21] M. Cook, D. Soloveichik, E. Winfree, and J. Bruck, "Programmability of chemical reaction networks," in *Algorithmic Bioprocesses*. Springer, 2009, pp. 543–584.

[22] M. Ş. Kuran, H. B. Yilmaz, T. Tugcu, and I. F. Akyildiz, "Interference effects on modulation techniques in diffusion based nanonetworks," *Nano Commun. Netw.*, vol. 3, no. 1, pp. 65–73, Mar. 2012.

[23] U. Alon, "Network motifs: Theory and experimental approaches," *Nature Rev. Genet.*, vol. 8, no. 6, pp. 450–461, Jun. 2007.

[24] M. Kuscu and O. B. Akan, "Modeling convection-diffusion-reaction systems for microfluidic molecular communications with surface-based receivers in Internet of bio-nano things," *PLoS ONE*, vol. 13, no. 2, Feb. 2018, Art. no. e0192202.

[25] R. W. Bradley, M. Buck, and B. Wang, "Recognizing and engineering digital-like logic gates and switches in gene regulatory networks," *Current Opinion Microbiol.*, vol. 33, pp. 74–82, Oct. 2016.

[26] K. Lee *et al.*, "Generalized serial dilution module for monotonic and arbitrary microfluidic gradient generators," *Lab Chip*, vol. 9, no. 5, pp. 709–717, 2009.

[27] G. M. Whitesides, "The origins and the future of microfluidics," *Nature*, vol. 442, no. 7101, pp. 368–373, Jul. 2006.

[28] G. Karlebach and R. Shamir, "Modelling and analysis of gene regulatory networks," *Nature*, vol. 9, no. 10, pp. 770–780, Oct. 2008.

[29] R. Milo, "Network motifs: Simple building blocks of complex networks," *Science*, vol. 298, no. 5594, pp. 824–827, Oct. 2002.

[30] A. Uri, *An Introduction to Systems Biology: Design Principles of Biological Circuits*. London, U.K.: Chapman & Hall, 2006.

[31] S. Mangan, S. Itzkovitz, A. Zaslaver, and U. Alon, "The incoherent feed-forward loop accelerates the response-time of the gal system of escherichia coli," *J. Mol. Biol.*, vol. 356, no. 5, pp. 1073–1081, Mar. 2006.

[32] L. J. Kahl and D. Endy, "A survey of enabling technologies in synthetic biology," *J. Biol. Eng.*, vol. 7, no. 1, p. 13, 2013.

[33] T. H. Klinge, "Modular and robust computation with deterministic chemical reaction networks," Ph.D. dissertation, Dept. Comput. Sci., Iowa State Univ., Ames, IA, USA, 2016.

[34] B. Wang, R. I. Kitney, N. Joly, and M. Buck, "Engineering modular and orthogonal genetic logic gates for robust digital-like synthetic biology," *Nature Commun.*, vol. 2, no. 1, pp. 1–9, Oct. 2011.

[35] X. J. Li and Y. Zhou, *Microfluidic Devices for Biomedical Applications*. Sawston, U.K.: Woodhead, 2013.

[36] D. Di Carlo, "Inertial microfluidics," *Lab Chip*, vol. 9, no. 21, pp. 3038–3046, Sep. 2009.

[37] T. Stocker, *Introduction to Climate Modelling*. Berlin, Germany: Springer, 2011.

[38] W. Wicke, T. Schwering, A. Ahmadzadeh, V. Jamali, A. Noel, and R. Schober, "Modeling duct flow for molecular communication," in *Proc. IEEE Global Commun. Conf. (GLOBECOM)*, Dec. 2018, pp. 206–212.

[39] A. O. Bicen and I. F. Akyildiz, "End-to-end propagation noise and memory analysis for molecular communication over microfluidic channels," *IEEE Trans. Commun.*, vol. 62, no. 7, pp. 2432–2443, Jul. 2014.

[40] W. Hundsdorfer and J. G. Verwer, *Numerical Solution of Time-Dependent Advection-Diffusion-Reaction Equations*. New York, NY, USA: Springer, 2013.

[41] Y.-A. Chen *et al.*, "Generation of oxygen gradients in microfluidic devices for cell culture using spatially confined chemical reactions," *Lab Chip*, vol. 11, no. 21, pp. 3626–3633, Sep. 2011.

[42] Y.-H. Chen, C.-C. Peng, Y.-J. Cheng, J.-G. Wu, and Y.-C. Tung, "Generation of nitric oxide gradients in microfluidic devices for cell culture using spatially controlled chemical reactions," *Biomicrofluidics*, vol. 7, no. 6, Nov. 2013, Art. no. 064104.

[43] H. Yang and M. A. M. Gijs, "Micro-optics for microfluidic analytical applications," *Chem. Soc. Rev.*, vol. 47, no. 4, pp. 1391–1458, 2018.

[44] Y. Deng, A. Noel, M. Elkashlan, A. Nallanathan, and K. C. Cheung, "Modeling and simulation of molecular communication systems with a reversible adsorption receiver," *IEEE Trans. Mol., Biol. Multi-Scale Commun.*, vol. 1, no. 4, pp. 347–362, Dec. 2015.

[45] J. G. Wendel, "The non-absolute convergence of gil-Pelaez' inversion integral," *Ann. Math. Statist.*, vol. 32, no. 1, pp. 338–339, Mar. 1961.

Massimiliano Pierobon (Member, IEEE) received the Ph.D. degree in electrical and computer engineering from the Georgia Institute of Technology, Atlanta, GA, USA, in 2013. Since August 2013, he has been an Assistant Professor with the Department of Computer Science and Engineering, University of Nebraska–Lincoln (UNL), NE, USA, where he also holds a courtesy appointment at the Department of Biochemistry. His research interests are in molecular communication theory, nanonetworks, intrabody networks, communication engineering applied to synthetic biology, and the Internet of Bio-Nano Things. His selected honors include the 2011 Georgia Tech BWN Lab Researcher of the Year Award, the 2013 IEEE Communications Letters Exemplary Reviewer Award, the UNL CSE Upper and Graduate Level Teaching Award in 2016 and 2017, the 2017 IEEE INFOCOM Best Paper Runner-Up Award, and the Best In-Session Presentation Award. He is currently the PI of the NSF Project WetComm: Foundations of Wet Communication Theory, a Co-PI of the NSF Project Redox-enabled Bio-Electronics for Molecular Communication and Memory (RE-BIONICS), and has been the lead PIs of the NSF project TelePathy: Telecommunication Systems Modeling and Engineering of Cell Communication Pathways. He has been the Co-Editor in Chief of *Nano Communication Networks* (Elsevier) since July 2017, and an Associate Editor of IEEE TRANSACTIONS ON COMMUNICATIONS from 2013 to 2020.

Dadi Bi (Student Member, IEEE) is currently pursuing the Ph.D. degree with the Department of Engineering, Kings College London, U.K. His research interests include molecular communication and microfluidics. He has served as a member of Technical Program Committees for the 2020 IEEE ICC. He received the Exemplary Reviewers of IEEE TRANSACTIONS ON COMMUNICATIONS in 2019.

Arumugam Nallanathan (Fellow, IEEE) was with the Department of Informatics, King's College London, from December 2007 to August 2017, where he was Professor of wireless communications from April 2013 to August 2017 and has been a Visiting Professor since September 2017. He was an Assistant Professor with the Department of Electrical and Computer Engineering, National University of Singapore, from August 2000 to December 2007. He has been a Professor of wireless communications and the Head of the Communication Systems Research (CSR) Group, School of Electronic Engineering and Computer Science, Queen Mary University of London, since September 2017. His research interests include artificial intelligence for wireless systems, beyond 5G wireless networks, the Internet of Things (IoT), and molecular communications. He has published nearly 500 technical papers in scientific journals and international conferences.

Prof. Nallanathan received the IEEE Communications Society SPCE Outstanding Service Award 2012 and IEEE Communications Society RCC Outstanding Service Award 2014. He was a co-recipient of the Best Paper Awards presented at the IEEE International Conference on Communications 2016 (ICC'2016), IEEE Global Communications Conference 2017 (GLOBECOM'2017), and IEEE Vehicular Technology Conference 2018 (VTC'2018). He has served as the Chair for the Signal Processing and Communication Electronics Technical Committee of IEEE Communications Society and the Technical Program Chair and a member of Technical Program Committees in numerous IEEE conferences. He is an IEEE Distinguished Lecturer. He has been selected as a Web of Science Highly Cited Researcher in 2016. He was an Editor of IEEE TRANSACTIONS ON WIRELESS COMMUNICATIONS from 2006 to 2011, IEEE TRANSACTIONS ON VEHICULAR TECHNOLOGY from 2006 to 2017, and IEEE SIGNAL PROCESSING LETTERS. He is an Editor of IEEE TRANSACTIONS ON COMMUNICATIONS and a Senior Editor of IEEE WIRELESS COMMUNICATIONS LETTERS.

Yansha Deng (Member, IEEE) received the Ph.D. degree in electrical engineering from the Queen Mary University of London, U.K., in 2015. From 2015 to 2017, she was a Post-Doctoral Research Fellow with the Kings College London, U.K., where she is currently a Lecturer (Assistant Professor) with the Department of Engineering. Her research interests include molecular communication, machine learning, and 5G wireless networks. She has served as a TPC Member for many IEEE conferences, such as IEEE GLOBECOM and ICC. She has received the Exemplary Reviewers of IEEE TRANSACTIONS ON COMMUNICATIONS in 2016 and 2017 and IEEE TRANSACTIONS ON WIRELESS COMMUNICATIONS in 2018. She was a recipient of the Best Paper Awards from ICC 2016 and Globecom 2017 as the first author. She is currently an Associate Editor of IEEE TRANSACTIONS ON COMMUNICATIONS and IEEE TRANSACTIONS ON MOLECULAR, BIOLOGICAL AND MULTI-SCALE COMMUNICATIONS, and a Senior Editor of IEEE COMMUNICATION LETTERS.